Microporous and Mesoporous Materials 151 (2012) 481–487

Contents lists available at SciVerse ScienceDirect

Microporous and Mesoporous Materials

journal homepage: www.elsevier.com/locate/micromeso

CO_2/CH_4, CH_4/H_2 and $CO_2/CH_4/H_2$ separations at high pressures using Mg_2(dobdc)

Zoey R. Herm, Rajamani Krishna *[,1], Jeffrey R. Long *

Department of Chemistry, University of California, Berkeley, CA 94720, USA

ARTICLE INFO

Article history:
Received 13 July 2011
Received in revised form 27 August 2011
Accepted 1 September 2011
Available online 10 September 2011

Keywords:
Metal–organic framework
Carbon capture
Mg_2(dobdc)
Hydrogen purification
Natural gas purification

ABSTRACT

High-pressure separations of binary and ternary mixtures of CO_2, CH_4, and H_2 are relevant to carbon dioxide capture as well as hydrogen and natural gas purification. Metal–organic frameworks represent a class of porous materials that could be used to accomplish these separations, and Mg_2(dobdc) (dobdc^{4-} = 1,4-dioxido-2,5-benzenedicarboxylate), also sometimes referred to as Mg–MOF-74 or CPO-27–Mg, is an especially lightweight metal–organic framework with a high concentration of coordinatively-unsaturated metal sites decorating its interior surfaces. High pressure CH_4 adsorption isotherms presented here, together with CO_2 and H_2 adsorption behavior, are analyzed using the Ideal Adsorbed Solution Theory to model CO_2/CH_4, CH_4/H_2, and $CO_2/CH_4/H_2$ mixture separations using Mg_2(dobdc). The selectivities, working capacities and breakthrough performances for these three mixtures are reported, and Mg_2(dobdc) is shown to outperform zeolite 13X in each scenario.

1. Introduction

The development of efficient new methods of separating gas mixtures into their component parts is urgently needed for two distinct reasons. First, many gas separations are performed on vast scales in numerous industrial processes and so improvements will lead to global energy savings [1]. Additionally, carbon capture and storage is an exciting possibility for preventing the release of anthropogenic carbon dioxide into the atmosphere and hinges on gas separations at its core. Current gas separation processes are not sufficiently advanced to render carbon capture a viable addition to power plants [2,3]. As a result, optimizing gas separations is a pragmatic approach to solving contemporary energy-related problems.

The adsorptive separation of gases, wherein one constituent interacts more strongly with the internal surfaces of a porous material, is a leading candidate in most gas separation applications [4]. This cyclic process exposes a gas mixture to a bed filled with porous adsorbent, through which one component moves quickly to the other end. The other gas adsorbs to the internal surface of the adsorbent, and is removed by either dropping the pressure or increasing the temperature to regenerate the bed [5]. Zeolites and activated carbons are common, established porous materials that offer the advantages of being inexpensive and already optimized for many existing gas separation processes.

The exceptional porosity and chemical tunability of metal–organic frameworks, a class of porous materials that has emerged relatively recently, render them exciting candidates to replace or augment the current suite of available adsorbents [6]. Because these materials are composed of multifunctional organic molecules linked by metal cations, a nearly limitless number of combinations are available to form new structures, resulting in an immense versatility in the possible geometries and surface properties. Ideally, a metal–organic framework could be synthesized specifically for application in any given gas separation [7].

1.1. High-pressure CO_2/CH_4, CH_4/H_2, and $CO_2/CH_4/H_2$ separations

Hydrogen purification is one industrial process for which optimized adsorbents are urgently needed. Over 50 million tons of H_2 are synthesized and purified annually [8], and the same process for generating hydrogen could potentially be a step in one method for reducing carbon dioxide emissions from power plants. In pre-combustion CO_2 capture, H_2 is isolated from the other gases present after its synthesis and prior to its combustion, rendering water as the only combustion product. Physisorptive separation using porous adsorbents, the strategy that is already performed in many H_2 purification plants [9], is attractive for both H_2 purification and pre-combustion CO_2 capture, since improvements to current processes will not require drastic engineering overhauls.

Hydrogen is commonly generated by steam-reforming of methane. This process generates CO and H_2. Using this CO, the water–gas shift reaction generates CO_2 and more H_2. Some CO (ca. 1–3%) and CH_4 (ca. 3–6%) impurities remain in addition to the large fraction of CO_2 (ca. 15–25%) [10]. Because such a large proportion

* Corresponding authors. Tel.: +1 510 642 0860; fax: +1 510 642 8369.
E-mail addresses: r.krishna@uva.nl (R. Krishna), jrlong@berkeley.edu (J.R. Long).
[1] Permanent address: Van't Hoff Institute for Molecular Sciences, University of Amsterdam, Science Park 904, 1098 XH Amsterdam, The Netherlands.

1387-1811/$ - see front matter © 2011 Elsevier Inc. All rights reserved.
doi:10.1016/j.micromeso.2011.09.004

of the resulting gas mixture is CO_2, an ideal adsorbent will have a high capacity for CO_2. However, the separation of CH_4 from H_2 is equally or perhaps more important than CO_2/H_2 separation. This is because in a packed bed of porous adsorbent the *least* adsorbing impurity will elute first and contaminate the product stream [11]. The adsorbent must be regenerated when an impurity starts to elute, and regeneration is a critical factor in optimizing an adsorptive purification system [12]. In an H_2 stream contaminated with CO_2, CH_4, and CO, CH_4 is the least adsorbing impurity, because it has no quadrupole or dipole moment [13]. Methane is also important to remove from a flue gas since it is a potent greenhouse gas [14].

The separation of CH_4 from H_2 is also relevant to refinery off-gas processing [13,15]. The gas mixture being separated is approximately 50% H_2 at 5–10 bar [16,17]. Here, the impurities are C1–C5 hydrocarbons. As in $CO_2/CH_4/H_2$ separation, the most difficult separation is the most important to optimize. Methane is the smallest of the impurities, making the van der Waals forces between it and the surface of a porous material the weakest [16]. As a result, CH_4/H_2 separation is the most difficult separation to achieve in refinery off-gas separation.

Separation of CO_2 from CH_4 is a distinct separation from those described above. It is relevant to the purification of natural gas, which can have up to 92% CO_2 impurity at its source [18]. Removal of CO_2, which is most commonly accomplished using amines [19] to reduce CO_2 levels to the required 2% maximum, is conducted between 20 and 70 bar [20]. Carbon dioxide removal is required for approximately 25% of the natural gas reserves in the United States [18].

1.2. The metal–organic framework Mg_2(dobdc)

Metal–organic frameworks are a class of porous materials that offer potential advantages over traditional adsorbents for all of the aforementioned gas separations. A number of these have already been studied for separations of CO_2/CH_4 [21–26], CH_4/H_2 [27–35], and CO_2/H_2 [11,31,32,36–45]. Frameworks featuring coordinatively-unsaturated metal sites are especially promising for these gas separations. High-pressure adsorption isotherms of CO_2 and CH_4 have been calculated [46,47] and measured [48] together in metal–organic frameworks of this type. High-pressure CO_2, H_2 and CH_4 adsorption behavior have been studied in isolation in even more metal–organic frameworks with open metal sites.

We recently reported that metal–organic frameworks are promising candidates for effecting H_2 separation from CO_2 and, as a result, are possible alternatives to current adsorbents (zeolites and activated carbons) for H_2 purification or pre-combustion CO_2 capture [42]. In particular, Mg_2(dobdc), a metal–organic framework with a high concentration of exposed Mg^{2+} sites decorating its surface, displayed a much higher CO_2/H_2 selectivity than other frameworks, as well as zeolites and activated carbons. Additionally, its working capacity (the difference in the amount adsorbed at the high adsorption pressure and the lower purge pressure) is much higher than activated carbons, zeolites, and most other metal–organic frameworks. Computationally, Mg_2(dobdc) was shown to be outstanding in both selectivity and CO_2 capacity among an even larger group of zeolites, activated carbons and metal–organic frameworks when compared for both CO_2/H_2 and CH_4/H_2 separations [45]. Experimentally, the material was investigated for the ambient-pressure separation of CO_2 and CH_4 in Mg_2(dobdc) [26] and high-pressure adsorption isotherms of CO_2 and CH_4 were also measured [49]. Both of these studies reported breakthrough curves for CO_2/CH_4 mixtures, but neither discussed the equilibrium mixture behavior.

In order to rigorously examine the applicability of Mg_2(dobdc) for CO_2/CH_4, CH_4/H_2, and $CO_2/CH_4/H_2$ separations, we now report pure-component CH_4 adsorption behavior onto Mg_2(dobdc). These data are analyzed together with the previously reported high-pressure CO_2 and H_2 isotherms [42]. Low pressure (0–1 bar) CO_2 and CH_4 adsorption isotherms are also reported in order to improve the quality of the data set. The Ideal Adsorbed Solution Theory (IAST) [50] is applied to pure component isotherms of CH_4, H_2 and CO_2 in order to demonstrate the selectivity and working capacity for binary CO_2/CH_4 and CH_4/H_2, as well as ternary $CH_4/H_2/CO_2$, mixtures. Breakthrough behavior for CO_2/CH_4, CH_4/H_2 and $CO_2/H_2/CH_4$ mixtures are simulated. All of the isotherms were measured on samples of Mg_2(dobdc) generated in the same laboratory and confirmed to be of high quality via cryogenic N_2 adsorption measurements, a technique that is very sensitive to the purity of the sample.

2. Experimental

2.1. Synthesis and characterization of Mg_2(dobdc)

The compound Mg_2(dobdc) was synthesized as reported previously [42]. All reagents were obtained from commercial vendors and used without further purification. The material was activated using a strategy adapted from the literature procedure. The yellow microcrystalline solids were combined and washed five times with DMF and soaked in DMF for 24 h. The DMF was decanted, and freshly distilled methanol was added. The solid was then transferred to a nitrogen-filled glovebox. The methanol was decanted and the solid was soaked in anhydrous DMF on a hotplate set at 100 °C for 18 h. The DMF was decanted and replaced, and the solid was soaked at 100 °C for 4 h. The DMF was decanted and replaced by methanol, which was decanted and replenished 12 times with a minimum of 6 h between washes. Infrared spectroscopy was used to confirm the removal of all DMF by monitoring the C=O stretch at ca. 1650 cm^{-1} (see Fig. S1). Infrared spectra were obtained on a Perkin–Elmer Spectrum 100 Optica FTIR spectrometer furnished with an attenuated total reflectance accessory (ATR).

2.2. Low-pressure gas adsorption measurements

Gas adsorption isotherms for pressures in the range 0–1.1 bar were measured by a volumetric method using a Micromeritics ASAP2020 instrument. A sample was transferred in an N_2-filled glovebox to a pre-weighed analysis tube, which was capped with a transeal and evacuated by heating to 180 °C at 0.1 °C per minute under dynamic vacuum for until the outgas rate was determined to be 4 μTorr/min. The evacuated analysis tube containing the degassed sample was then carefully transferred to an electronic balance and weighed again to determine the mass of sample. The tube was then transferred back to the analysis port of the gas adsorption instrument. For all isotherms, warm and cold free space correction measurements were performed using ultra-high purity He gas (UHP grade 5.0, 99.999% purity); N_2 isotherms at 77 K were measured in liquid nitrogen using UHP-grade gas sources. Adsorption of CO_2 and CH_4 at 323 K was measured using a Julabo isothermal bath with UHP-grade gases. Oil-free vacuum pumps and oil-free pressure regulators were used for all measurements to prevent contamination of the samples during the evacuation process or of the feed gases during the isotherm measurements.

2.3. High-pressure gas adsorption measurements

A sample of Mg_2(dobdc) (289.0 mg) was loaded in an air-free sample holder in a glove box under a nitrogen atmosphere. The stainless steel sample holder was weighed five times before adding the sample and three times afterwards in order to determine the

precise mass of Mg_2(dobdc). Methane excess adsorption measurements were performed on an automated Sieverts' apparatus (PCT-Pro-E&E from Setaram Instrumentation) over a pressure range of 1–50 bar. UHP grade 5.0 methane and helium (99.999% purity) were used. Total adsorption was calculated using NIST Thermochemical Properties of Fluid Systems [51]: CH_4 densities between 0 and 50 bar were fit using a sixth-order polynomial, then multiplied by the previously reported pore volume of 0.57 cm^3/g. The Langmuir region of the 77 K N_2 adsorption isotherm was measured again after the high-pressure adsorption measurement to ensure sample contamination had not occurred (see Fig. S2).

2.4. Ideal Adsorbed Solution Theory calculations

The Ideal Adsorbed Solution Theory (IAST) of Prausnitz and Myers was used to estimate the composition of the adsorbed phase from pure component isotherm data [50,52]. A detailed explanation of the IAST calculations has been previously reported [42]. The pure component isotherm data for CO_2, CH_4, and H_2 in Mg_2(dobdc), after conversion to absolute loadings, were fitted with Langmuir–Freundlich isotherm models. For the cases of CO_2 and CH_4 dual-site isotherm models of the type shown in Eq. (1) were employed.

$$q_i = q_{i,A,sat}\frac{b_{i,A}p_i^{\nu_{i,A}}}{1+b_{i,A}p_i^{\nu_{i,A}}} + q_{i,B,sat}\frac{b_{i,B}p_i^{\nu_{i,B}}}{1+b_{i,B}p_i^{\nu_{i,B}}} \quad (1)$$

Here, q_i is the component molar loading of species i (in mol/kg), $q_{i,sat}$ is the saturation loading of species i and p_i is the bulk gas pressure of species i (in Pa). Subscripts A and B refer to the two different types of adsorption sites on the surface. The parameters ν_i are the dimensionless exponent in the Langmuir–Freundlich isotherms. These parameters are provided for all three gases in Table 1. For the case of H_2, the data were fit using a single-site isotherm model in which the second term in Eq. (1) is dropped. Fig. S3 compares the experimental data with the Langmuir–Freundlich fits.

2.5. Zeolite 13X data treatment

The pure component isotherm data for CO_2, CH_4, and H_2 in zeolite 13X were obtained from previous reports [53,54]. In cases where the excess loadings were reported, these were converted to absolute loadings using the reported pore volume data along with the Peng–Robinson equation of state for estimation of fluid densities in the pores. The reported data are for a variety of temperatures that unfortunately do not include 313 K. In these cases the Langmuir constants were fitted using Eq. (2).

$$b_{i,A} = b_{i,A0}\,exp\left(\frac{E}{RT}\right)$$
$$b_{i,B} = b_{i,A0}\,exp\left(\frac{E}{RT}\right) \quad (2)$$

Here, b is the dual-site Langmuir–Freundlich constant for species i and A and B represent the two adsorption sites on the surface. The heats of adsorption, E, for CO_2, CH_4, and H_2 were taken to be 35, 14, and 6 kJ/mol respectively. The reported values of the dual-site Langmuir–Freundlich parameters are listed in Table 1 and are for T = 313 K. Figs. S4 and S5 compare the experimental data with the dual-site Langmuir–Freundlich fits for 313 K.

2.6. Breakthrough simulations

The methods employed for performing breakthrough simulations have been described in detail elsewhere [11].

3. Results and discussion

3.1. Pure-component CO_2, CH_4, and H_2 adsorption in Mg_2(dobdc)

Fig. 1 shows the pure-component absolute adsorption isotherms for CH_4, H_2, and CO_2 in Mg_2(dobdc) at 313 K and pressures in the range 0–40 bar. These isotherms are in agreement with previously published data [3,42,49]. At 35 bar, CO_2 has reached saturation at 15 mmol/g, while CH_4 and H_2 have not, reaching ca. 10 and 3 mmol/g, respectively. The H_2 adsorption isotherm is linear in this pressure window, while CH_4 begins to approach saturation behavior.

These isotherms were fit with Langmuir–Freundlich models using a dual-site model for CO_2 and CH_4 and a single-site model for H_2 (see Table 1). The open-metal sites in Mg_2(dobdc) create heterogeneity in the surface that requires this type of modeling; however, the small size and low adsorption enthalpy of H_2 led to a sufficiently good fit of the data using a single-site model.

3.2. CO_2/CH_4, CH_4/H_2 and $CO_2/CH_4/H_2$ separations calculated with IAST

The remainder of this article discusses the mixed-gas adsorption behavior of CO_2, CH_4, and H_2 in Mg_2(dobdc). Using the Ideal Adsorbed Solution Theory (IAST) [50], mixed-gas adsorption behavior was extracted from the pure-component isotherms. Such estimations are essential in practice because collecting experimental data on mixture adsorption is time consuming and extremely rare [55]. IAST was used to calculate selectivity, working capacity and breakthrough performance.

The binary mixtures are calculated as a 50/50 composition. This composition was chosen because most reports of these mixtures employ a 50/50 mixture. Further, this ratio should mitigate some of the artifacts of IAST that can be observed when the less-adsorbed species is a large fraction of the gas mixture [44]. The ternary mixture is 1:4:20 CH_4:CO_2:H_2 in an effort to model a realistic hydrogen purification composition.

The use of IAST with any adsorbent/adsorbate mixture system must be carefully considered due to the limitations of the theory [56]. We have determined IAST to be appropriate for the gas mixtures evaluated here. The theory has been used to evaluate CH_4/H_2 [30], CO_2/CH_4 [25,57–63], and CO_2/H_2 [42] gas mixtures in metal–organic frameworks. More valuable in evaluating the validity of IAST in these gas mixtures are comparisons of IAST and Grand Canonical Monte Carlo (GCMC) simulations. It has been show that IAST compares well with GCMC simulations of CH_4/H_2 selectivity

Table 1
Dual-site Langmuir–Freundlich parameters for pure CH_4, H_2 and CO_2 data for Mg_2(dobdc) and zeolite 13X at 313 K.

		Site A			Site B		
		$q_{i,A,sat}$ (mol/kg)	$b_{i,A}$, $Pa^{-\nu_i}$	$n_{i,A}$ Dimensionless	$q_{i,B,sat}$ (mol/kg)	$b_{i,B}$,$Pa^{-\nu_i}$	$n_{i,A}$ Dimensionless
CO_2	Mg_2(dobdc)	6.8	2.48×10^{-4}	1	9.9	1.4×10^{-6}	1
	13X	3.5	2.51×10^{-7}	1	5.2	4.16×10^{-5}	1
CH_4	Mg_2(dobdc)	11	7.91×10^{-7}	1	5	1.9×10^{-8}	1
	13X	4	7.92×10^{-8}	1	5	8.12×10^{-7}	1
H_2	Mg_2(dobdc)	40	1.62×10^{-7}	0.832			
	13X	18	2.43×10^{-8}	1			

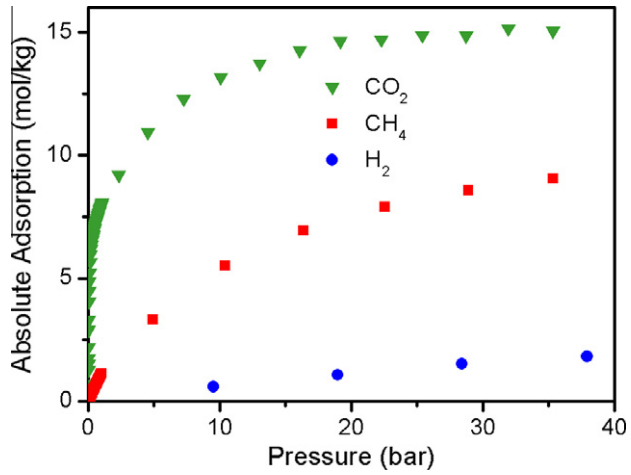

Fig. 1. Absolute adsorption isotherms for CO_2, CH_4 and H_2 in Mg_2(dobdc) at 313 K. (For interpretation of the references to color in this figure legend, the reader is referred to the web version of this article.)

in MOF-5 and HKUST-1 [32]. The effectiveness of IAST has also been validated by this method for CH_4/H_2 separations in non-interpenetrated [29,31,33,34] and interpenetrated [35,64] metal–organic frameworks. GCMC simulations have further validated the use of IAST for the modeling of CO_2/CH_4 mixtures in metal–organic frameworks [64–66]. Finally, the use of IAST for CO_2/H_2 separations has been validated in Mg_2(dobdc) specifically using configurational bias Monte Carlo simulations [67].

3.3. CO_2/CH_4, CH_4/H_2 and $CO_2/CH_4/H_2$ selectivity

Selectivity is an important metric for evaluating adsorbents and can be calculated using IAST [68,69]. Selectivity for a binary gas mixture is defined as in Eq. (3), where q_i is the mole fraction of component i in the adsorbed phase and p_i is the mole fraction of component i in the bulk gas phase.

$$\text{Selectivity} = \frac{q_1/q_2}{p_1/p_2} \tag{3}$$

Fig. 2 shows CO_2/CH_4, CH_4/H_2 and $(CO_2 + CH_4)/H_2$ selectivities for Mg_2(dobdc). CO_2/H_2 selectivity is also shown for comparison for an 80:20 mixture. As expected, the CO_2/CH_4 selectivity is higher than the CH_4/H_2 selectivity, and both are lower than the CO_2/H_2 selectivity, which ranges from 900–400 at these pressures [42]. This can be rationalized using the quadrupole moments and polarizabilities of the three gases [13] and are discussed individually below.

CO_2/CH_4 selectivity is high because CH_4 has no quadrupole moment, while CO_2 does. In contrast, CO_2/H_2 selectivity is higher than CO_2/CH_4 because CO_2 is has a higher quadrupole moment and higher polarizability than H_2, while CO_2 and CH_4 have similar polarizabilities. The selectivity decreases drastically for the CO_2/CH_4 mixture up to 5 bar, which can be attributed to the strong CO_2 binding at low loadings evidenced by the steep rise in the pure-component isotherm at low pressures [38].

CH_4/H_2 selectivity is the lowest selectivity examined here because while CH_4 is more polarizable than H_2 the quadrupole moment of H_2 is *larger* than that of CH_4. However, the difference in quadrupole moment between CH_4 and H_2 is larger (6.62×10^{25} esu cm^2) than the difference in polarizability (17.888×10^{25} cm^3).

The selectivity for three-component $CH_4/CO_2/H_2$ mixtures relevant to hydrogen purification and pre-combustion CO_2 capture is also shown in Fig. 2. In a 1:4:20 CH_4:CO_2:H_2 mixture, the selectivity for both CO_2 and CH_4 decreases from 1400 at 1 bar to 260 at 40 bar. This selectivity is slightly lower than the 20:80 CO_2:H_2 selectivity reported in an earlier work [42]. This is expected, as compared to a 20:80 mixture a 4:16:80 CH_4:CO_2:H_2 mixture essentially replaces a fraction of strongly-selective CO_2 with less-selective CH_4.

Because of the variability in gas mixture compositions in the shifted products of steam-methane reforming, refinery off-gas, and natural gas, investigating the performance under different compositions is an important indicator of a broadly useful material. Fig. 3 shows the selectivity for CH_4 in a CH_4/H_2 mixture and mixture as a function of mole fraction of CH_4. Selectivity for CH_4 in a CH_4/H_2 mixture varies only slightly with composition at all pressures. This is expected because the selectivity shown in Fig. 2 is not strongly pressure-dependent and therefore should not be dependent on the partial pressure of CH_4.

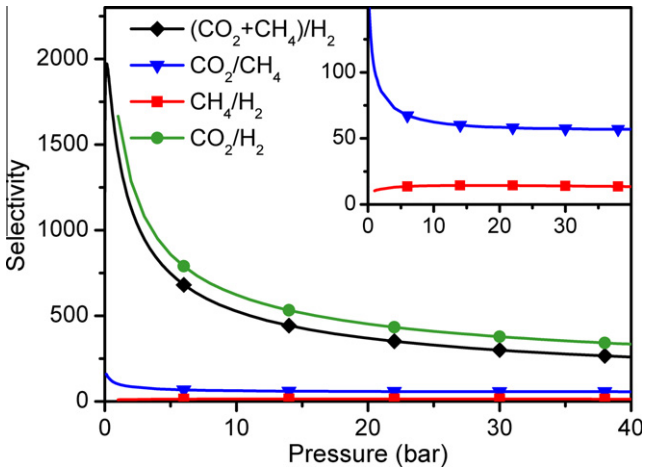

Fig. 2. IAST selectivities obtained for Mg_2(dobdc) at 313 K for CO_2 and CH_4 in a 1:4:20 CH_4:CO_2:H_2 mixture, CO_2 in a 1:1 CO_2:CH_4 mixture, CH_4 in a 1:1 CH_4:H_2 mixture and CO_2 in an 80:20 H_2:CO_2 mixture. Selectivities are calculated throughout the entire line trace, and symbols are only shown to distinguish the lines visually. (For interpretation of the references to color in this figure legend, the reader is referred to the web version of this article.)

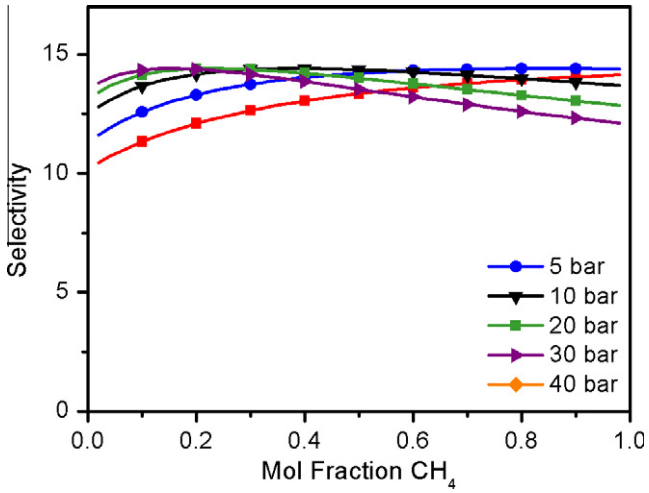

Fig. 3. IAST selectivities obtained for Mg_2(dobdc) at 313 K for CH_4 in a 1:1 CH_4:H_2 mixture at 5, 10, 20, 30 and 40 bar. Selectivities are calculated throughout the entire line trace, and symbols are only shown to distinguish the lines visually. (For interpretation of the references to color in this figure legend, the reader is referred to the web version of this article.)

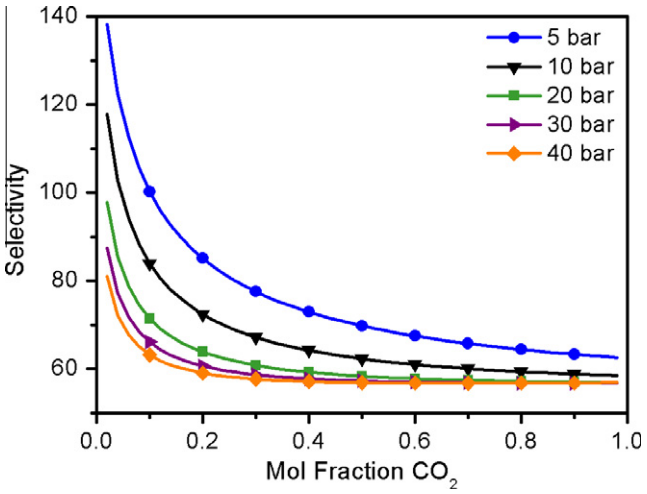

Fig. 4. IAST selectivities obtained for Mg_2(dobdc) at 313 K for CO_2 in a 1:1 CO_2:CH_4 mixture at 5, 10, 20, 30 and 40 bar. Selectivities are calculated throughout the entire line trace, and symbols are only shown to distinguish the lines visually. (For interpretation of the references to color in this figure legend, the reader is referred to the web version of this article.)

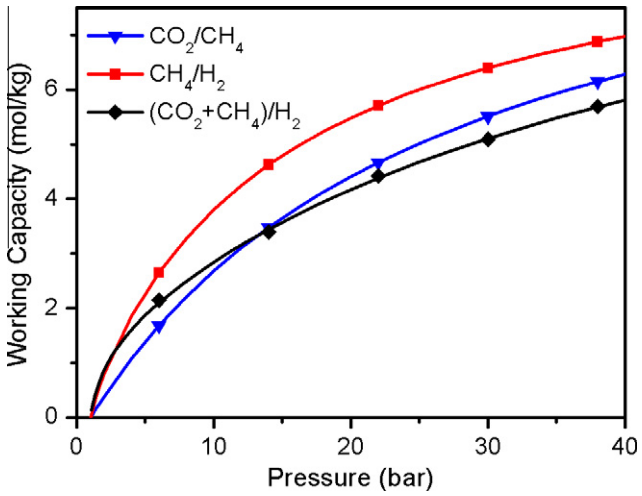

Fig. 5. IAST-calculated gravimetric working capacities for Mg_2(dobdc) at 313 K assuming a purge pressure of 1 bar for CO_2 and CH_4 in a 1:4:20 CH_4:CO_2:H_2 mixture, CO_2 in a 1:1 CO_2:CH_4 mixture, and CH_4 in a 1:1 CH_4:H_2 mixture. Working capacities are calculated throughout the entire line trace, and symbols are only shown to distinguish the lines visually. (For interpretation of the references to color in this figure legend, the reader is referred to the web version of this article.)

Fig. 4 shows the selectivity for CO_2 in a CO_2/CH_4 as a function of mole fraction of CO_2. In contrast to CH_4/H_2 selectivity, which is nearly pressure-independent, CO_2/CH_4 selectivity decreases by half from 2% to 98% CO_2 in the case of a 5 bar mixture. This is expected because selectivity decreases with higher partial pressures of CO_2 due to the saturation of the strongly adsorbing sites on the surface of Mg_2(dobdc). At high mole fractions of CO_2, the selectivity asymptotically approaches ca. 57.

3.4. CO_2/CH_4, CH_4/H_2 and CO_2/CH_4/H_2 working capacity

The working capacity of Mg_2(dobdc) for these same three mixtures can be seen in Fig. 5. The working capacity is the difference between the amount adsorbed at high pressures and the amount adsorbed at the lower purge pressure, which is assumed here to be 1 bar. It has been previously reported [68,69] that the working capacity is equally as important as selectivity in optimizing an adsorbent for pressure-swing adsorption. The working capacity of CO_2 is higher than for CH_4, but the difference is smaller than the difference in the pure-component isotherms. This is a result of the shallow rise in adsorption of CH_4 at lower pressures. The three-component mixture working capacity falls close to the binary mixture capacities but is lower at high pressures. This can be attributed to the difference in compositions of the three mixtures studied, as 80% of the mixture is comprised of H_2 in the three-component mixture.

3.5. CO_2/CH_4, CH_4/H_2 and CO_2/CH_4/H_2 breakthrough performance

The performance of a pressure swing adsorber, an industrial gas separation unit that relies on physisorption at high pressure and regeneration at low pressure, is dictated by both selectivity and capacity considerations. In a recent publication, we developed a procedure for screening MOFs using transient breakthrough of gas mixtures in a fixed bed adsorber [11]. In this approach, a dimensionless breakthrough time is defined and calculated assuming isothermal conditions. The breakthrough time, for a specified purity of the outlet gas mixtures, represents an appropriate combination of selectivity and capacity that is relevant in practice. In the current work, we use the same approach to evaluate the performance of Mg_2(dobdc).

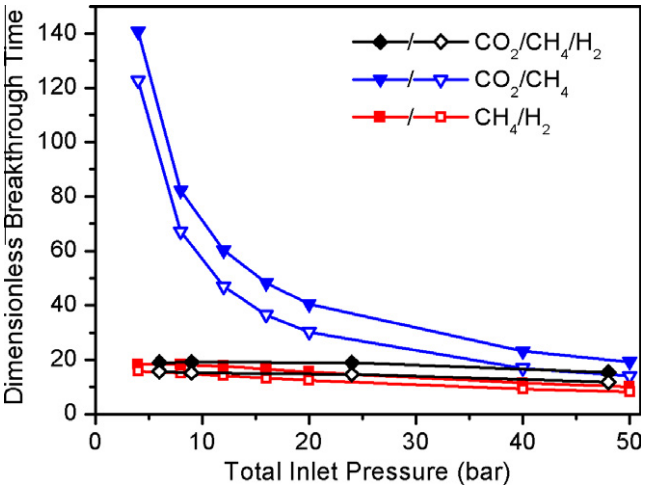

Fig. 6. Dimensionless breakthrough times at 313 K for a 1:1:1 CH_4:CO_2:H_2 mixture, 1:1 CO_2:CH_4, and a 1:1 CH_4:H_2 mixture as a function of the inlet pressure of a packed bed adsorber where the breakthrough is defined as 0.05 mol percent impurity in outlet gas. Closed symbols represent Mg_2(dobdc) and open symbols represent zeolite 13X. Lines are for visualization purposes only. (For interpretation of the references to color in this figure legend, the reader is referred to the web version of this article.)

Fig. 6 displays the time at which 0.05 mol percent of the gas leaving the column is impurity gas for equimolar mixtures of CO_2/CH_4, CH_4/H_2, and CO_2/CH_4/H_2 in both Mg_2(dobdc) and zeolite 13X. Interestingly, CH_4/CO_2/H_2 and CH_4/H_2 mixture breakthrough times are very similar and CO_2/CH_4 breakthrough times are much higher. This difference can theoretically be attributed to the significantly lower adsorption strength of H_2.

Fig. 7 displays the amount of CO_2 or CH_4 that is adsorbed by the time this breakthrough threshold is reached. The relative ordering of the three separations is dependent on the ratios of less-adsorbing to more-adsorbing compounds. CO_2/CH_4 mixtures display a high breakthrough capacity due to the high breakthrough time paired with the high working capacity for CO_2 in Mg_2(dobdc). CH_4/H_2 is lower due to the lower breakthrough time, despite the similar work-

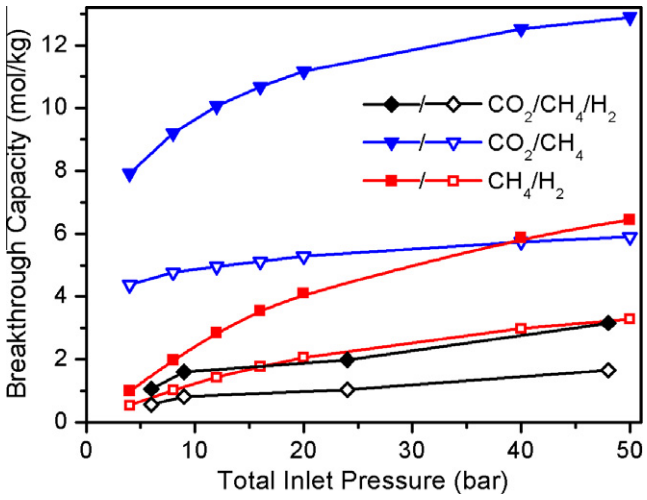

Fig. 7. Adsorption capacity for CO_2 at 313 K in a 1:1:1 CH_4:CO_2:H_2 mixture and 1:1 CO_2:CH_4 and CH_4 in a 1:1 CH_4:H_2 mixture as a function of the inlet pressure of a packed bed adsorber where the breakthrough is defined as 0.05 mol percent impurity in outlet gas. Closed symbols represent Mg_2(dobdc) and open symbols represent zeolite 13X. Lines are for visualization purposes only. (For interpretation of the references to color in this figure legend, the reader is referred to the web version of this article.)

ing capacity. The $CO_2/CH_4/H_2$ breakthrough capacity shows only the amount of CO_2 adsorbed rather than both CO_2 and CH_4, illustrating the reduction in CO_2 adsorption in the presence of other gases.

3.6. CO_2/CH_4, CH_4/H_2 and $CO_2/CH_4/H_2$ selectivity, working capacity and breakthrough performance in zeolite 13X compared to Mg_2(dobdc)

Figs. S6–S9 display the selectivity and working capacity of zeolite 13X using the same analysis scenarios described above for Mg_2(dobdc) and shown in Figs. 2–5. This zeolite was chosen for comparison because it has an exceptionally high CO_2 capacity [70] and breakthrough performance [71] compared to other zeolites. High-pressure adsorption isotherms for CO_2, CH_4, and H_2 in zeolite 13X have been reported previously [53].

In every case, Mg_2(dobdc) outperforms zeolite 13X. The three selectivities shown in Fig. S6 resemble those in Fig. 2, but are 75–50% lower. The three working capacity traces are approximately half of those of Mg_2(dobdc). Fig. S7 shows the CH_4/H_2 selectivity displays a clear trend of decreasing selectivity between 10 and 6 from 2% to 98% CH_4. This can preliminarily be ascribed to a modestly higher pressure dependence in CH_4/H_2 selectivity for zeolite 13X compared to Mg_2(dobdc). Fig. S8 displays the CO_2/CH_4 selectivity decreases with increasing CO_2 partial pressure, here approaching a value of 20 rather than 57.

The working capacity of zeolite 13X is approximately half that of Mg_2(dobdc) for all separations evaluated. In all three cases of breakthrough adsorption, Mg_2(dobdc) adsorbs approximately double the amount of gas as zeolite 13X with slightly higher breakthrough times. The difference in working capacity can explain this behavior. The supporting information includes video animations of the breakthrough behavior of 1:1 CO_2:CH_4 and CH_4:H_2 mixtures and a 1:1:1 CH_4:CO_2:H_2 mixture for both Mg_2(dobdc) and zeolite 13X. In all of these high pressure breakthrough cases, Mg_2(dobdc) outperforms zeolite 13X significantly.

4. Conclusions

Here, we have presented the experimental single-component CH_4 adsorption behavior of Mg_2(dobdc). Together with previously reported CO_2 and H_2 isotherms, we experimentally evaluated this material for high-pressure gas separations performance. Binary CO_2/CH_4 and CH_4/H_2 as well as ternary $CO_2/CH_4/H_2$ mixtures were examined by applying the Ideal Adsorbed Solution Theory to these pure component isotherms. The selectivity and working capacity of Mg_2(dobdc) render this material promising for all of these high pressure separations, where it offers significant improvements over the competing material zeolite 13X. Further work on the industrial applicability of Mg_2(dobdc) could involve substantiating prior calculations wherein the use of Mg_2(dobdc) as a membrane for high pressure gas separations was investigated [67].

Additionally, experimentally evaluating Mg_2(dobdc) for its performance under regeneration conditions is pertinent. We expect Mg_2(dobdc) to perform as well or better than zeolite 13X due to the isosteric heat of adsorption of CO_2 onto the two materials. Between 0 and 6 mmol/g, zeolite 13X decreases from approximately 50 to 37 kJ/mol [72], where Mg_2(dobdc) decreases from approximately 42 to 38 kJ/mol [3]. More specifically, the strengths of the interaction at the assumed purge pressure of 1 bar are 46 and 41 kJ/mol for zeolite 13X and Mg_2(dobdc), respectively. At higher loadings, the heat of adsorption on Mg_2(dobdc) decreases even further after a steep drop in heat at 8 mmol/g where 1 CO_2 per Mg^{2+} site is achieved. Despite the promising regeneration capability these data suggest, laboratory regeneration experiments are necessary to determine the usefulness of this material in an industrial setting.

Acknowledgements

This research was funded through the Center for Gas Separations Relevant to Clean Energy Technologies, an Energy Frontier Research Center funded by the US Department of Energy, Office of Science, Office of Basic Energy Sciences under Award No. DE-SC0001015.

Appendix A. Supplementary data

Supplementary data associated with this article can be found, in the online version, at doi:10.1016/j.micromeso.2011.09.004.

References

[1] R.T. Yang, Adsorbents: Fundamentals and Applications, Wiley-Interscience, Hoboken, 2003.
[2] S. Chu, Science 325 (2009) 1599.
[3] J.A. Mason, K. Sumida, Z.R. Herm, R. Krishna, J.R. Long, Energy Environ. Sci. 4 (2011) 3030–3040.
[4] R.T. Yang, Gas Separation by Adsorption Processes, Imperial College Press, London, 1996.
[5] M.D. LeVan, G. Carta, Adsorption and ion exchange, in: D.W. Green (Ed.), Perry's Chemical Engineers' Handbook, McGraw-Hill, New York, 2008, pp. 1–69.
[6] A.U. Czaja, N. Trukhan, U. Müller, Chem. Soc. Rev. 38 (2009) 1284–1293.
[7] B. Chen, S. Xiang, G. Qian, Acc. Chem. Res. 43 (2010) 1115–1124.
[8] C.-J. Winter, Int. J. Hydrogen Energy 30 (2005) 681–685.
[9] A. Damle, Hydrogen separation and purification, in: R.B. Gupta (Ed.), Hydrogen Fuel: Production, Transport and Storage, CRC Press, Boca Raton, 2009, pp. 283–326.
[10] S. Sircar, T.C. Golden, Sep. Sci. Technol. 35 (2000) 667–687.
[11] R. Krishna, J.R. Long, J. Phys. Chem. C 115 (2011) 12941–12950.
[12] A.M. Ribeiro, C.A. Grande, F.V.S. Lopes, J.M. Loureiro, A.E. Rodrigues, Chem. Eng. Sci. 63 (2008) 5258–5273.
[13] J.-R. Li, R.J. Kuppler, H.-C. Zhou, Chem. Soc. Rev. 38 (2009) 1477–1504.
[14] L. Loulergue, A. Schilt, R. Spahni, V. Masson-Delmotte, T. Blunier, B. Lemiuex, J.-M. Barnola, D. Raynaud, T.F. Stocker, J. Chappellaz, Nature 453 (2008) 383–386.
[15] C. Voss, Adsorption 11 (2005) 527–529.
[16] M.B. Rao, S. Sircar, J. Membr. Sci. 85 (1993) 253–264.
[17] A. Malek, S. Farooq, AIChE J. 44 (1998) 1985–1992.
[18] W.R. Parrish, A.J. Kidnay, Overview of the natural gas industry, in: Fundamentals of Natural Gas Processing, CRC Press, Boca Raton, 2006, pp. 10–11.
[19] S.R. Venna, M.A. Carreon, Langmuir 27 (2011) 2888–2894.

[20] W.R. Parrish, A.J. Kidnay, Gas treating, in: Fundamentals of Natural Gas Processing, CRC Press, Boca Raton, 2006, p. 93.
[21] L. Bastin, P.S. Bárcia, E.J. Hurtado, J.A.C. Silva, A.E. Rodrigues, B. Chen, J. Phys. Chem. C 112 (2008) 1575–1581.
[22] M. Eddaoudi, J. Kim, N. Rosi, D. Vodak, J. Watcher, M. O'Keeffe, O.M. Yaghi, Science 295 (2002) 469–472.
[23] S. Bourrelly, P.L. Llewellyn, C. Serre, F. Millange, T. Loiseau, G. Férey, J. Am. Chem. Soc. 127 (2005) 13519–13521.
[24] Y.-S. Bae, K.L. Mulfort, H. Frost, P. Ryan, S. Punnathanam, L.J. Broadbelt, J.T. Hupp, R.Q. Snurr, Langmuir 24 (2008) 8592–8598.
[25] B. Mu, F. Li, K.S. Walton, Chem. Commun. (2009) 2493–2495.
[26] D. Britt, H. Furukawa, B. Wang, T.G. Glover, O.M. Yaghi, Proc. Natl. Acad. Sci. USA 106 (2009) 20637–20640.
[27] M. Gallo, D. Mitnik-Glossman, J. Phys. Chem. C 113 (2009) 6634–6642.
[28] B. Liu, Q. Yang, C. Xue, C. Zhong, B. Chen, B. Smit, J. Phys. Chem. C 112 (2008) 9854–9860.
[29] J. Liu, J.K. Johnson, J. Low, Temp. Phys. 157 (2009) 268–276.
[30] S. Keskin, D.S. Sholl, Ind. Eng. Chem. Res. 48 (2009) 914–922.
[31] Y. Liu, D. Liu, Q. Yang, C. Zhong, J. Mi, Ind. Eng. Chem. Res. 49 (2010) 2902–2906.
[32] Q. Yang, C. Zhong, J. Phys. Chem. B 110 (2006) 17776–17783.
[33] S. Keskin, Ind. Eng. Chem. Res. 49 (2010) 11689–11696.
[34] S. Keskin, J. Liu, J.K. Johnson, D.S. Sholl, Langmuir 24 (2008) 8254–8261.
[35] B. Liu, C.Y. Sun, G.J. Chen, Chem. Eng. Sci. 66 (2011) 3012–3019.
[36] J. Jiang, AIChE J. 55 (2009) 2422–2432.
[37] R. Babarao, M. Eddauodi, J.W. Jiang, Langmuir 26 (2010) 11196–11203.
[38] R. Babarao, J.W. Jiang, Ind. Eng. Chem. Res. 50 (2011) 62–68.
[39] R. Babarao, J. Jiang, J. Am. Chem. Soc. 131 (2009) 11417–11425.
[40] D. Wu, Q. Xu, D. Liu, C. Zhong, J. Phys. Chem. C 113 (2010) 16611–16617.
[41] Y. Chen, J. Jiang, ChemSusChem 3 (2010) 982–988.
[42] Z.R. Herm, J.A. Swisher, B. Smit, R. Krishna, J.R. Long, J. Am. Chem. Soc. 133 (2011) 5664–5667.
[43] Q. Yang, Q. Xu, B. Liu, C. Zhong, B. Smit, Chin. J. Chem. Eng. 17 (2009) 781–790.
[44] S. Keskin, J. Phys. Chem. C 115 (2011) 800–807.
[45] R. Krishna, J.M. van Baten, Phys. Chem. Chem. Phys. 13 (2011) 10593–10616.
[46] R. Babarao, J. Jiang, S.I. Sandler, Langmuir 25 (2009) 5239–5247.
[47] Q. Xu, D. Liu, Q. Yang, C. Zhong, J. Mi, J. Mater. Chem. 20 (2010) 706–714.
[48] P.L. Llewellyn, S. Bourrelly, C. Serre, A. Vimont, M. Daturi, L. Hamon, G.D. Weireld, J.-S. Chang, D.-Y. Hong, Y.K. Hwang, S.H. Jhung, G. Férey, Langmuir 24 (2008) 7245–7250.
[49] P.D.C. Dietzel, V. Besikiotis, R. Blom, J. Mater. Chem. 19 (2009) 7362–7370.
[50] A.L. Myers, J.M. Prausnitz, AIChE J. 11 (1965) 121–127.
[51] E.W. Lemmon, M.O. McLinden, D.G. Friend, NIST chemistry WebBook, Nist standard reference database number 69, in: P.J. Linstrom, W.G. Mallard (Eds.), Thermophysical Properties of Fluid Systems, National Institute of Standards and Technology, Gaithersburg, 2010.
[52] C. Tien, Adsorption Calculations and Modeling, Butterworth–Heineman, Boston, 1994.
[53] Y. Belmabkhout, G. Pirngruber, E. Jolimaitre, A. Methivier, Adsorption 13 (2007) 341–349.
[54] S. Cavenati, C.A. Grande, A.E. Rodrigues, J. Chem. Eng. Data 49 (2004) 1095–1101.
[55] O. Talu, Adv. Colloid Interface Sci. 77 (1998) 227–269.
[56] S. Keskin, J. Liu, R.B. Rankin, J.K. Johnson, D.S. Sholl, Ind. Eng. Chem. Res. 48 (2009) 2355–2371.
[57] Y.-S. Bae, O.K. Farha, A.M. Spokoyny, C.A. Mirkin, J.T. Hupp, R.Q. Snurr, Chem. Commun. (2008) 4135–4137.
[58] Y.-S. Bae, A.M. Spokoyny, O.K. Farha, R.Q. Snurr, J.T. Hupp, C.A. Mirkin, Chem. Commun. 46 (2010) 3478–3480.
[59] J.-B. Lin, W. Xue, J.-P. Zhang, X.-M. Chen, Chem. Commun. 47 (2011) 926–928.
[60] Y.-S. Bae, B.G. Hauser, O.K. Farha, J.T. Hupp, R.Q. Snurr, Microporous Mesoporous Mater. 141 (2011) 231–235.
[61] Z. Bao, S. Alnemrat, L. Yu, I. Vasiliev, Q. Ren, X. Lu, S. Deng, J. Colloid Interface Sci. 357 (2011) 504–509.
[62] J. Erucar, S. Keskin, J. Phys. Chem. C 115 (2011) 13637–13644.
[63] J.Y. Lee, J.M. Roberts, O.K. Farha, A.A. Sarjeant, K.A. Scheidt, J.T. Hupp, Inorg. Chem. 48 (2009) 9971–9973.
[64] B. Liu, B. Smit, J. Phys. Chem. C 114 (2010) 8515–8522.
[65] R. Babarao, Z. Hu, J. Jiang, S. Chempath, S.I. Sandler, Langmuir 23 (2007) 659–666.
[66] S. Keskin, Ind. Eng. Chem. Res. 50 (2011) 8230–8236.
[67] R. Krishna, J.M. van Baten, J. Membr. Sci. 377 (2011) 249–260.
[68] R. Kumar, Ind. Eng. Chem. Res. 33 (1994) 1600–1605.
[69] M.T. Ho, G.W. Allinson, D.E. Wiley, Adsorption 47 (2008) 4883–4890.
[70] D. Bonenfant, M. Kharoune, P. Niquette, M. Mimeault, R. Hausler, Sci. Technol. Adv. Mater. 9 (2008) 1–7.
[71] P.D. Jadhav, S.S. Rayalu, R.B. Biniwale, S. Devotta, Curr. Sci. 92 (2007) 724–726.
[72] F.R. Siperstein, A.L. Myers, AIChE J. 47 (2001) 1141–1159.